

Temperature dependent effective mass renormalization in 2D electron systems

S. Das Sarma, Victor M. Galitski, and Ying Zhang
Condensed Matter Theory Center, Department of Physics,
University of Maryland, College Park, MD 20742-4111
(Dated: October 29, 2018)

We calculate, as a function of temperature and density, the electron-electron interaction induced quasiparticle effective mass renormalization in 2D electron systems within the leading-order dynamically screened Coulomb interaction expansion. We find an unexpected nonanalyticity and nonmonotonicity in the temperature dependent effective mass with the renormalized mass linearly increasing with temperature at low temperatures for all densities.

PACS numbers: 71.10.-w; 71.10.Ca; 73.20.Mf; 73.40.-c

I. INTRODUCTION

A key insight of the Landau Fermi Liquid theory is that interactions in a Fermi system lead to the renormalization of the single particle fermion mass giving rise to “quasiparticles” with renormalized effective mass whose low energy behavior is qualitatively similar to the corresponding noninteracting free particles^{1,2}. Then, various single particles properties, e.g. specific heat, density of states, etc., in the interacting Fermi system are simply given, at least in the leading-order theory, by replacing the bare (i.e. “free particle”) mass m by the corresponding renormalized effective mass m^* . In this paper we present the very *first* microscopic calculation of the *temperature dependent* effective mass renormalization in an interacting 2D electron system (2DES), finding in the process an unexpected nonanalytic and nonmonotonic behavior of the effective mass $m^*(T)$ as a function of temperature in the 2DES. In particular, $m^*(T)$ first increases linearly with temperature in a 2DES reaching a density dependent maximum around $T/T_F \lesssim 0.1 - 0.5$, where T_F is the noninteracting Fermi temperature, after which it decreases with increasing temperature. This nonmonotonic behavior, in particular the temperature induced enhancement of the 2DES quasiparticle effective mass at low temperatures, is entirely unexpected because the naive expectation is that quantum many-body electron-electron interaction effects (underlying the effective mass renormalization phenomenon) should decrease with increasing temperature since the high temperature system is necessarily a classical system. The nonanalytic linear- T dependence of $m^*(T)$ is also quite unexpected since the usual fermionic Sommerfeld thermal expansion always results in a quadratic temperature correction.

Our work is partially motivated by the great deal of recent activity in semiconductor-based 2DES, e.g. Si inversion layers, GaAs heterostructures and quantum wells, etc. where the 2D carrier density can be varied (by tuning an external gate voltage), modifying the strength of the electron-electron interaction usually measured^{1,2} by the dimensionless parameter $r_s = me^2/(\hbar^2\sqrt{\pi n})$ with n being the 2D carrier density and m the bare (i.e. band) mass. The r_s -parameter¹ in 3D metals (defined with respect to 3D densities) is typically 3 – 5 whereas in

semiconductor 2DES r_s could vary from 1 (or less) to 20 (or higher), depending on the specific semiconductor system and carrier density being studied. Since the effective mass renormalization scales with r_s (small and large r_s respectively corresponding to weakly and strongly interacting electron systems), one expects interesting and important many-body quasiparticle renormalization in 2DES, particularly at large r_s . It is therefore not surprising that the issue of the effective mass renormalization in 2DES has been extensively studied, both experimentally³ and theoretically^{5,6,7,8,9} over the last thirty years. All these theoretical studies of quasiparticle mass renormalization have, however, been restricted to $T = 0$ both in the 2D^{5,6,7,8,9} and 3D¹⁰ system. While this zero-temperature restriction makes perfect sense in 3D systems where the relevant Fermi temperature $T_F = E_F/k_B$ (defining the temperature scale for the electron system) is extremely high ($T_F \sim 10^4 K$ in metals), it makes little sense for extremely low density 2DES of current interest^{11,12,13} where $T_F \lesssim 1K$, making $T/T_F \sim 1$ in the experimental temperature range. The temperature (and density) dependent effective mass renormalization calculation presented in this paper therefore takes on additional significance because a number of recent experiments have reported large 2D effective mass renormalization^{11,12,13} at low densities and low temperatures. We note in this context that the 2D effective mass renormalization m^*/m in our finite temperature many-body theory is a function of two dimensionless parameter r_s ($\propto n^{-1/2}$) and T/T_F ($\propto n^{-1}$, since $k_B T_F = \pi \hbar^2 n/m$ in 2DES), which are however *not* completely independent of each other (since they both depend on the electron density)—in particular, $T/T_F \sim r_s^2$ for a fixed temperature and changing density.

The structure of this paper goes as following: In section II we present the theory for our effective mass calculation. In section III we provide our numerical results of our calculated effective mass as a function of r_s and T . In section IV we present the analytical results for effective mass in the $r_s \ll 1$ and $T/T_F \ll 1$ limit. We conclude in section V with a brief discussion.

II. THEORY

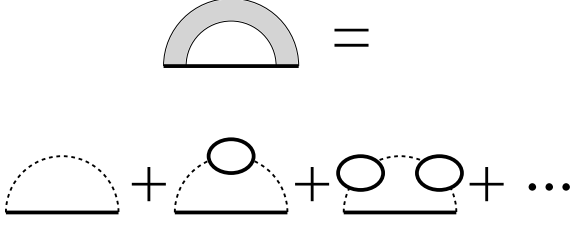


FIG. 1: The Feynman diagram for the self-energy. The circles are polarization bubbles, the dashed lines the Coulomb interaction, and the solid lines the electron Green's function.

We consider a 2DES interacting via the long range Coulomb interaction. The effective mass renormalization is microscopically calculated² from the electron self-energy function $\Sigma(\mathbf{k}, i\nu_l)$ defined at the Matsubara imaginary frequency $i\nu_l$ and 2D wavevector \mathbf{k} . To calculate the electron self-energy, we make the well-known ‘‘GW’’ approximation^{5,10,14} of a leading order expansion in the dynamically screened Coulomb interaction (the corresponding Feynman diagram for the self-energy is shown in Fig. 1), obtaining ($\hbar = 1$ throughout):

$$\Sigma(\mathbf{k}, i\nu_l) = - \int \frac{d^2q}{(2\pi)^2} T \sum_{\omega_n} \frac{V_q}{\epsilon(\mathbf{q}, i\omega_n)} \times \frac{1}{i\nu_l + i\omega_n - \xi_{\mathbf{q}-\mathbf{k}}}, \quad (1)$$

where $V_q = 2\pi e^2/q$ is the 2D bare Coulomb potential, $i\nu_l = i(2l+1)\pi k_B T$ and $i\omega_n = i2n\pi k_B T$ are the usual fermion/boson odd/even Matsubara frequencies (l, n integers), $\xi_{\mathbf{k}} = k^2/(2m) - \mu$, μ the chemical potential, and $\epsilon(\mathbf{k}, i\omega_n)$ is the RPA dynamical dielectric function, given by the sum of the polarization bubble diagrams:

$$\epsilon(\mathbf{k}, i\omega_n) = 1 - V_q \Pi(\mathbf{k}, i\omega_n), \quad (2)$$

with $\Pi(\mathbf{k}, i\omega_n)$ the electronic 2D polarizability. Within RPA, we have

$$\Pi(\mathbf{k}, i\omega_n) = 2 \int \frac{d^2q}{(2\pi)^2} \frac{n_F(\xi_{\mathbf{q}}) - n_F(\xi_{\mathbf{q}-\mathbf{k}})}{\xi_{\mathbf{q}} - \xi_{\mathbf{q}-\mathbf{k}} + i\omega_n}, \quad (3)$$

where $n_F(x) = 1/(e^{x/T} + 1)$ is the Fermi distribution function.

The form of retarded polarizability $\Pi(\mathbf{k}, \omega) \equiv \Pi(\mathbf{k}, i\omega_n \rightarrow \omega + i0^+)$ has been provided by previous work⁴ at zero temperature:

$$\Pi_0(\mathbf{k}, \omega, \mu) = -\frac{m}{\pi} + \frac{m^2}{\pi k^2} \left[\sqrt{\left(\omega + \frac{k^2}{2m}\right)^2 - \frac{2\mu k^2}{2m}} - \sqrt{\left(\omega - \frac{k^2}{2m}\right)^2 - \frac{2\mu k^2}{2m}} \right], \quad (4)$$

where μ is the chemical potential. The finite temperature form of retarded polarizability can be obtained from Eq. (4) by

$$\Pi(\mathbf{k}, \omega, \mu; T) = \int_0^\infty d\mu' \frac{\Pi_0(\mathbf{k}, \omega, \mu')}{4T \cosh^2(\frac{\mu' - \mu}{2T})}. \quad (5)$$

The quasiparticle energy $E_{\mathbf{k}}$ is obtained from the Dyson equation using the analytically continued retarded self-energy $\Sigma(\mathbf{k}, i\nu_l \rightarrow \omega + i0^+) \equiv \Sigma(\mathbf{k}, \omega)$:

$$E_{\mathbf{k}} = \xi_{\mathbf{k}} + \text{Re}\Sigma(\mathbf{k}, E_{\mathbf{k}}). \quad (6)$$

Eq.(6) is exact, while our GW-approximation is the first order perturbation expansion in the dynamically screened interaction. There has been much discussion on whether one should use exact Eq. (6) for the effective mass or the so-called on-shell approximation, keeping only first order interaction terms by taking the first order iteration of Eq. (6):

$$E_{\mathbf{k}} = \xi_{\mathbf{k}} + \text{Re}\Sigma(\mathbf{k}, \xi_{\mathbf{k}}). \quad (7)$$

The on-shell approximation is expected to be more accurate within the GW scheme as it effectively accounts for some vertex corrections and obeys the Ward identities. This approach has previously been used in 2D⁵ and 3D¹⁰ zero-temperature effective mass calculations, and is regarded to be better than solving the full Dyson equation (Eq. (6) above). The two approaches are identical in the high-density limit $r_s \ll 1$. For $r_s > 1$, they give qualitatively similar but quantitatively different results. The effective mass can then be derived from the relation $1/m^* = (k^{-1}dE_{\mathbf{k}}/dk)|_{k=k_F}$, remembering that the bare band mass m is given by $1/m = (k^{-1}d\xi_{\mathbf{k}}/dk)|_{k=k_F}$:

$$\frac{m^*}{m} = \left[1 + \frac{m}{k} \frac{d}{dk} \text{Re}\Sigma(k, \xi_k) \right]^{-1} \Big|_{k=k_F} \quad (8)$$

where k_F is the Fermi momentum for the non-interacting 2DES.

We use three different techniques in calculating the self-energy: frequency sum, frequency integration, and plasmon-pole approximation. The first two techniques are equivalent to each other, and correspond to different ways of doing the analytic continuation of the imaginary frequency self-energy. The frequency sum technique is explained in Ref.¹⁵, and the frequency integration technique, also called spectral representation, in Ref.². In the frequency sum method, the retarded self-energy is given

by

$$\begin{aligned} \text{Re}\Sigma(\mathbf{k}, \omega) = & - \int \frac{d^2q}{(2\pi)^2} V_q n_F(\xi_{\mathbf{q}-\mathbf{k}}) \\ & - \int \frac{d^2q}{(2\pi)^2} V_q \text{Re} \left[\frac{1}{\epsilon(q, \xi_{\mathbf{q}-\mathbf{k}} - \omega)} - 1 \right] \\ & \quad \times [n_B(\xi_{\mathbf{q}-\mathbf{k}} - \omega) + n_F(\xi_{\mathbf{q}-\mathbf{k}})] \\ & - \int \frac{d^2q}{(2\pi)^2} T \sum_{\omega_n} V_q \left[\frac{1}{\epsilon(q, i\omega_n)} - 1 \right] \\ & \quad \times \frac{1}{i\omega_n - (\xi_{\mathbf{q}-\mathbf{k}} - \omega)}, \end{aligned} \quad (9)$$

where $n_B(x) = 1/(e^{x/T} - 1)$ is the Bose distribution function. For the frequency integration method, the retarded self-energy is

$$\begin{aligned} \text{Re}\Sigma(\mathbf{k}, \omega) = & - \int \frac{d^2q}{(2\pi)^2} V_q n_F(\xi_{\mathbf{q}-\mathbf{k}}) \\ & - \int \frac{d^2q}{(2\pi)^2} \int \frac{d\nu}{2\pi} 2V_q \text{Im} \frac{1}{\epsilon(q, \nu)} \\ & \quad \times \frac{n_B(\nu) + n_F(\xi_{\mathbf{q}-\mathbf{k}})}{\nu - (\xi_{\mathbf{q}-\mathbf{k}} - \omega)}. \end{aligned} \quad (10)$$

The plasmon-pole approximation (PPA) is a simpler technique^{6,16,17} for carrying out the frequency sum in the RPA self-energy calculation by using a spectral pole (i.e. a delta function) ansatz for the dynamical dielectric function $\epsilon(\mathbf{k}, \omega)$:

$$\text{Im}\epsilon^{-1}(\mathbf{k}, \omega) = C_k [\delta(\omega - \bar{\omega}_k) - \delta(\omega + \bar{\omega}_k)] / 2, \quad (11)$$

where the spectral weight C_k and the pole $\bar{\omega}_k$ of the PPA propagator in Eq. (11) are determined by using the Kramers-Krönig relation (i.e. causality) and the f -sum rule (i.e. current conservation). We mention that $\bar{\omega}_k$ in Eq. (11) does *not* correspond to the real plasmon dispersion in the 2DES, but simulates the whole excitation spectra of the system behaving as an effective plasmon at low momentum and as the single-particle electron-hole excitation at large momentum, as constrained by the Kramers-Krönig relation and the f -sum rule. Details on the PPA are available in literature^{6,16}, including the finite-temperature generalization¹⁷. The PPA, which is known^{6,16,17} to give results close to the full RPA calculation of self-energy, allows a trivial carrying out of the frequency sum in the retarded self-energy function leading to:

$$\begin{aligned} \text{Re}\Sigma(\mathbf{k}, \omega) = & - \int \frac{d^2q}{(2\pi)^2} V_q n_F(\xi_{\mathbf{q}-\mathbf{k}}) \\ & - \int \frac{d^2q}{(2\pi)^2} V_q C_q \left[\frac{n_B(\bar{\omega}_q) + n_F(\xi_{\mathbf{q}-\mathbf{k}})}{\bar{\omega}_q - (\xi_{\mathbf{q}-\mathbf{k}} - \omega)} \right. \\ & \quad \left. + \frac{n_B(-\bar{\omega}_q) + n_F(\xi_{\mathbf{q}-\mathbf{k}})}{\bar{\omega}_q + (\xi_{\mathbf{q}-\mathbf{k}} - \omega)} \right]. \end{aligned} \quad (12)$$

We calculate the self-energy by carrying out the 2D momentum integration (Eq. 9, 10, 12) as well as the

frequency sum (Eq. 9) and the frequency integral (Eq. 10) in order to obtain the quasiparticle effective mass (Eq. 8). We emphasize that our reason for carrying out our calculation of the electron self-energy by three different techniques (RPA frequency sum and integration, and PPA) is to completely ensure the numerical accuracy of the calculated temperature dependent effective mass by comparing the consistency among the three sets of results. This is particularly significant since there is no existing temperature-dependent effective mass calculation in the literature for us to compare with. The fact that our three sets of results are consistent with each other (and we reproduce the existing^{5,6,7,8,9} $T = 0$ effective mass results from our finite temperature theory) provides compelling support for our conclusions in this paper. Since our results obtained in the three techniques are in good agreement, we will only show here our effective mass results using RPA frequency sum method for the sake of brevity.

III. NUMERICAL RESULTS

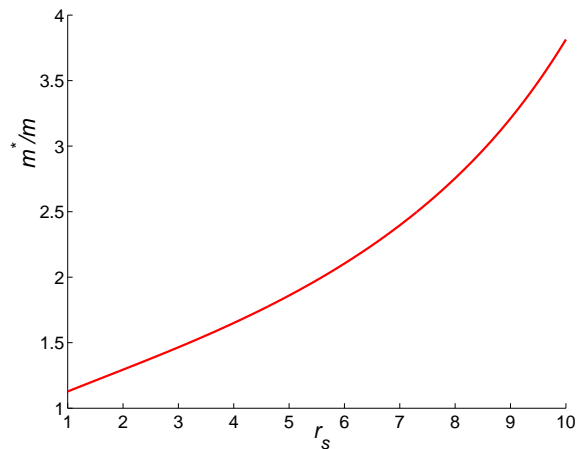


FIG. 2: Calculated $T=0$ effective mass as a function of r_s in a 2DES in the high r_s region.

First, we present our extreme low temperature 2D result ($T/T_F \approx 10^{-4}$) in Fig. 2 and Fig. 3, to be compared with the existing $T = 0$ 2D results^{5,6,7,8,9}, for $m^*(r_s)$ in the $r_s = 0 - 10$ range, showing that the effective mass renormalization could be almost as large as 5 for dilute $r_s \sim 10$ 2DES. We emphasize that the results presented in Fig. 2 and Fig. 3 based on the $T \rightarrow 0$ limit of our finite temperature theory are in *quantitative* agreement with the existing $T = 0$ 2D RPA effective mass calculations⁵ which were, however, restricted to the $r_s (< 5)$ regime.

In Fig. 4 we show our calculated 2D $m^*(T)$ as a function of T/T_F for different values of the 2D interaction parameter r_s ($= 1 - 10$). Fig. 5 shows the effective mass temperature dependence at high densities. In the low

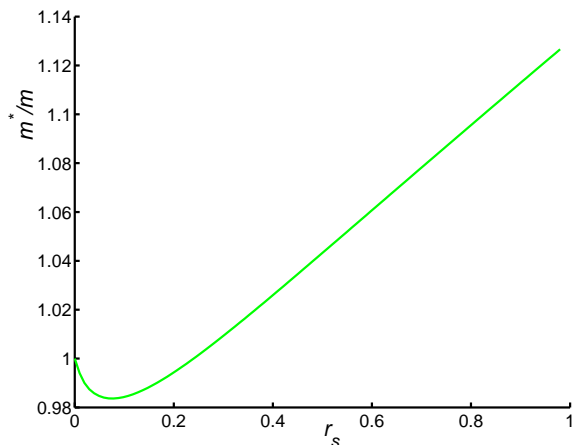


FIG. 3: Calculated $T=0$ effective mass as a function of r_s in a 2DES in the low r_s region.

temperature region the effective mass first rises to some maximum, and then decreases as temperature increases. This peculiar behavior is present at all densities. The nonmonotonic trend is systematic, and the value of T/T_F where the effective mass peaks increases with increasing r_s . The initial increase of $m^*(T)$ is linear in T/T_F as $T \rightarrow 0$, and the slope $\frac{d(m^*/m)}{d(T/T_F)}$ is almost independent of r_s for very small r_s (< 1), but increases with r_s for larger r_s values. We mention that we get somewhat stronger temperature dependence (i.e. larger dm^*/dT) in our PPA calculation (not shown here).

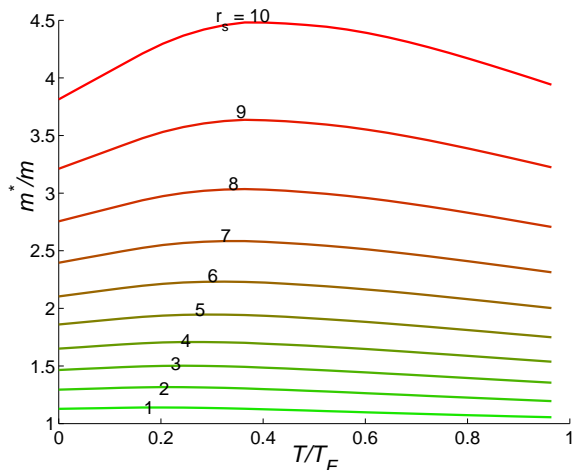


FIG. 4: Calculated 2D effective mass as a function of T/T_F for different high r_s values: $r_s = 10 \rightarrow 1$ from top to bottom. Note that $T_F \propto r_s^{-2}$, making the absolute temperature scale lower for higher r_s values.

In Fig. 6 we show the dependence of the effective mass renormalization as a function of the interaction parameter r_s for a few values of *fixed* temperature (rather than fixed T/T_F , remembering that $T_F \propto r_s^{-2}$ since $T_F \propto n$ and $r_s \propto n^{-1/2}$). The calculated $m^*(r_s)$ for fixed T val-

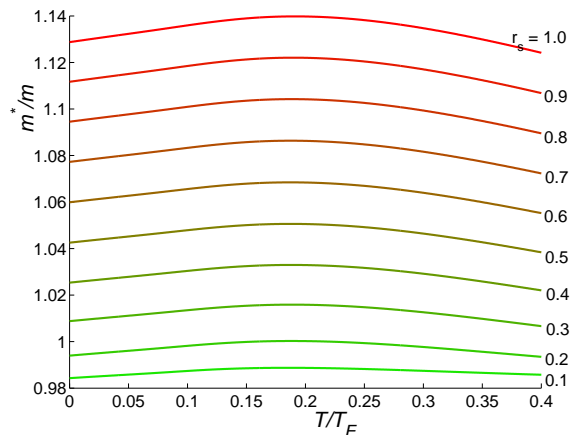


FIG. 5: Calculated 2D effective mass as a function of T/T_F for different low r_s values: $r_s = 1 \rightarrow 0.1$ from top to bottom.

ues is quite striking: For low fixed values of T , m^*/m initially increases with r_s even faster than the corresponding $T = 0$ result, eventually decreasing with r_s at large enough values (where the corresponding T/T_F values become large enough). This nonmonotonic behavior of $m^*(r_s)$ as a function of r_s for fixed temperatures showing a temperature-dependent maximum (with the value of r_s at which the m^* peak occurs decreasing with increasing T as in Fig. 6) is complementary to the nonmonotonicity of $m^*(T)$ in Fig. 4 as a function of T/T_F (at fixed r_s) and arises from the relationship between the dimensionless variables T/T_F ($\propto r_s^{-2}$) and r_s ($\propto T_F^{-1/2}$) due to their dependence on the carrier density (i.e. $T_F \propto n$ and $r_s \propto n^{-1/2}$).

One immediate consequence of our results shown in Figs. 4 and 6 is that $m^*(T/T_F, r_s) \equiv m^*(T, n)$ in 2DES could show a strong enhancement at low (but finite) temperatures and low electron densities (large r_s). Comparing with the actual system parameters for 2D electrons in Si inversion layers^{11,12} and GaAs heterostructures¹³ (and taking into account the quasi-2D form factor effects⁹ neglected in our strictly 2D calculation) we find that, consistent with recent experimental findings^{11,12,13}, our theoretical calculations predict (according to Figs. 4 and 6 as modified by subband form factors) m^*/m to be enhanced by a factor of 2–4 for the experimental densities and temperatures used in recent measurements^{11,12,13}. Due to the approximate nature of our theory we do not further pursue the comparison with experimental data in this paper leaving that for a future study.

IV. ANALYTICAL RESULTS IN $r_s \ll 1, T/T_F \ll 1$ LIMIT

We have also carried out an analytic calculation of the temperature-dependent 2D effective mass in the leading order dynamically screened interaction. This turns out to be an extremely difficult task due to the highly compli-

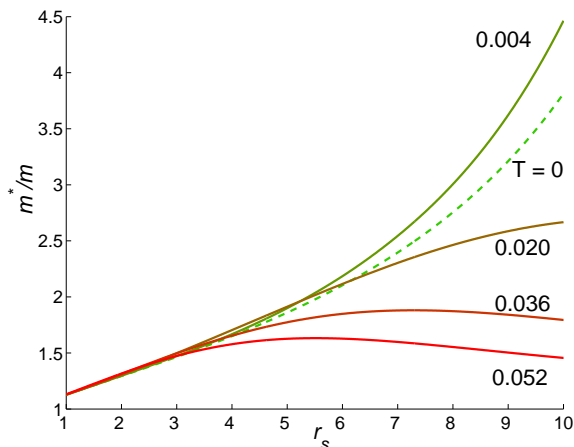


FIG. 6: Calculated m^*/m at fixed values of temperatures. T is in the units of T_F at $r_s = 1$.

cated nonanalytic structure of the integrand in Eq. (1), or equivalently Eqs. (9) or (10). It is only possible to carry out our analytical work in the high-density ($r_s \ll 1$), low temperature ($T/T_F \ll 1$) limit. It is well established that at zero temperature one can do an r_s expansion for the quasiparticle self-energy in the $r_s \ll 1$ limit since the leading order contribution in r_s comes only from the ring diagrams, which are exactly what we calculated in our theory (Fig. 1). In this sense, RPA is *exact* in the high-density limit, and one can calculate an exact quasiparticle effective mass from the diagrams of Fig. 1 in the $r_s \rightarrow 0$ limit. In the current work we carry out an exact expansion in the $r_s \rightarrow 0$ and $T/T_F \rightarrow 0$ limit. At finite temperatures, our analysis shows that it is valid to expand self-energy and effective mass in r_s and T/T_F in the $r_s \ll 1, T/T_F \ll 1$ region. Again we prove that the leading order contribution in r_s and T/T_F also only comes from the ring diagrams, and therefore RPA remains *exact* in this limit. Our calculation shows that

$$\frac{m^*}{m} = A(r_s) + B(r_s) \left(\frac{T}{T_F} \right) + C(r_s) \left(\frac{T}{T_F} \right)^2 \ln \left(\frac{T_F}{T} \right), \quad (13)$$

where $A(r_s)$, $B(r_s)$ and $C(r_s)$ are functions independent of temperature, and $B(r_s) \approx B_0 > 0$ and $C(r_s) < 0$ for $r_s \ll 1$.

In Eq. (13) the first term $A(r_s)$ is responsible for the nonmonotonic behavior of r_s dependence of m^* at zero temperature, i.e. when $T = 0, r_s \ll 1$, effective mass first decreases with increasing r_s , and then increases. This corresponds to our zero temperature effective mass curve as a function of r_s in $r_s \ll 1$ region, which is shown in Fig. 3. We mention here that this nonmonotonic zero temperature r_s dependence of the effective mass has already been found by previous works^{5,6,7,8,9}.

The second term in Eq. (13) accounts for the leading-order temperature correction to the effective mass, which is of more interest to us. Our analytical calculation shows that $B(r_s) \approx B_0 > 0$ for $r_s \ll 1$, ensuring that

the leading-order temperature correction, in agreement with our numerical results, enhances the effective mass renormalization in a linear manner as $T \rightarrow 0$. Moreover, the linear temperature coefficient is independent of r_s as $r_s \ll 1$ is also in good agreement with our numerical results in this region, as shown in Fig. 5 and discussed in section III.

The subleading temperature correction, shown as the third term in Eq. (13), is negative. This correction, combining with the leading order linear temperature correction, produces the peak in the effective mass temperature dependence. This again agrees qualitatively very well with our numerical findings in the $r_s \ll 1, T/T_F \ll 1$ region as shown in Fig. 5. Of course it is very difficult to determine whether the subleading temperature correction is T^2 or $T^2 \ln T$ dependence just by examining the numerical results, but the sign of this correction is certainly negative.

V. CONCLUSION

Our most important new result is the unanticipated non-analytic linear- T enhancement of the quasiparticle effective mass at low T/T_F and for *all* densities. This result transcends our specific GW approximation scheme since it persists for $r_s \ll 1$ where our approximation is exact. Since all quantum many-body renormalization must vanish in the classical high temperature limit, it follows rigorously that $m^*(T)$ must be nonmonotonic with a peak somewhere at an intermediate temperature as shown in Fig. 4. We point out, however, that this non-monotonicity would not be easy to observe experimentally since the quasiparticle is unlikely to be well-defined at finite values of T/T_F ($\sim 0.2 - 0.8$) where the peak of $m^*(T)$ lies. On the other hand, it should be possible to experimentally verify our predicted non-analytic linear in T enhancement of the quasiparticle effective mass at low T/T_F .

Finally, we comment on the approximations used in our calculation. First, our theory leaves out quasi-2D form factor (and related solid state physics) effects which are straightforward to include⁹ by appropriately modifying the bare interaction V_q in the theory, and would not lead to any qualitative changes in the results (but would reduce the magnitude of the mass renormalization by a factor of 1.2 to 2 depending on the electron density). Second (and more importantly), our use of the leading-order GW-RPA approximation, which is exact only in the high density ($r_s \ll 1$) limit, is open to question. Although we believe that at finite temperatures the GW-RPA approximation becomes more accurate (and our quasiparticle energy calculation of Eq. (3) approximately incorporates some vertex corrections going beyond the leading order expansion in the dynamically screened interaction^{5,10}), our principal rationale for carrying out the GW-RPA many-body calculation is that (a) it is the *only systematic* many-body perturbative calculation that is feasible

for interacting quantum Coulomb systems; and (b) RPA, while being exact only in the weakly interacting $r_s \ll 1$ limit, is known to produce qualitatively reasonable results even in the strongly interacting ($r_s > 1$) regime, as demonstrated by the agreement between RPA and experiments in 3D metals ($r_s \approx 3 - 5$) and in 2D semiconductor systems ($r_s \approx 1 - 10$). The fact that our predicted nonanalytic low temperature many-body enhancement of effective mass systematically persists to the $r_s \ll 1$ regime shows the generic validity of our results. In addition, RPA self-energy calculation should become more accurate as r_s increases (i.e. decreasing density) for a fixed non-zero T because RPA is exact at any density for

$T/T_F \gg 1$.

In this context we emphasize that the RPA self-energy calculation (i.e. our effective mass calculation based on the diagrams of Fig. 1) is an expansion in the dynamically screened Coulomb interaction which becomes equivalent to an expansion in r_s only in the $r_s \rightarrow 0$ limit. The RPA self-energy at arbitrary r_s may *not* be an expansion in r_s at all, but in some other effective parameters. Even in the high-density $r_s \rightarrow 0$ limit, the effective expansion parameter turn out to be r_s/γ where γ is a number of order 15(5) in 3(2) dimensional systems.

This work is supported by NSF-ECS, ONR, DARPA, and LPS.

-
- ¹ D. Pines and P. Nozieres, *The Theory of Quantum Liquids*, (Benjamin, New York, 1966).
- ² A. A. Abrikosov, L. P. Gor'kov, and I. E. Dzyaloshinski, *Methods of Quantum Field Theory in Statistical Physics*, (Prentice-Hall, Englewood Cliffs, 1963).
- ³ J. L. Smith and P. J. Stiles, Phys. Rev. Lett. **29**, 102 (1972); W. Pan, D. C. Tsui, B. L. Draper, Phys. Rev. B **59**, 10208 (1999).
- ⁴ F. Stern, Phys. Rev. Lett. **18**, 546 (1967).
- ⁵ C. S. Ting, T. K. Lee, and J. J. Quinn, Phys. Rev. Lett. **34**, 870 (1975).
- ⁶ B. Vinter, Phys. Rev. Lett. **35**, 1044 (1975).
- ⁷ R. Jalabert and S. Das Sarma, Phys. Rev. B **40**, 9723 (1989).
- ⁸ H. J. Schulze, P. Schuck, and N. Van Giai, Phys. Rev. B **61**, 8026 (2000).
- ⁹ T. Ando, A. B. Fowler, and F. Stern, Rev. Mod. Phys. **54**, 437 (1982).
- ¹⁰ T. M. Rice, Ann. Phys. (N. Y.) **31**, 100 (1965).
- ¹¹ A. A. Shashkin *et al.*, Phys. Rev. B **66**, 073303 (2002).
- ¹² A. A. Shashkin *et al.*, cond-mat/0302004; cond-mat/0301187.
- ¹³ J. Zhu *et al.*, Phys. Rev. Lett. **90**, 056805 (2003).
- ¹⁴ L. Hedin, Phys. Rev. **139**, A796 (1965); J. J. Quinn and R. A. Ferrell, *ibid.* **112** 812 (1958).
- ¹⁵ B. Y. K. Hu, Phys. Rev. B **47**, 1687 (1993); B. Y. K. Hu and S. Das Sarma, *ibid.* **48**, 5469 (1993).
- ¹⁶ B. I. Lundqvist, Phys. Kondens. Mater. **6**, 206 (1967).
- ¹⁷ S. Das Sarma *et al.*, Phys. Rev. B **19**, 6397 (1979).